# Nonlinear seismic fragility analysis of a resilient precast post-tensioned segmental bridge pier

*Ehsan Ahmadi[1], Sedef Kocakaplan[2], Mohammad M. Kashani[3]**
*[1]Faculty of Engineering and the Built Environment, Birmingham City University, UK*
*[2]Faculty of Engineering and Natural Sciences, Bursa Technical University, TR*
*[3]Faculty of Engineering and Physical Sciences, University of Southampton, UK*

** Corresponding Author, email: mehdi.kashani@soton.ac.uk*



## Abstract

The use of precast post-tensioned segmental (PPS) piers is growing in bridge industry, particularly in Accelerated Bridge Construction (ABC). The PPS piers provides durable, low-maintenance and demountable accelerated bridge construction technique that could be resilient to natural hazards. To expand their application in seismic regions, it is essential to investigate the behaviour of the PPS piers subject to various types of ground motions. Hence, this study focuses on the seismic performance of the PPS piers under pulse-like near-field earthquakes. Two ensembles of 40 pulse-like near-field ground motions and 44 far-field ground motions along with three bridge piers of various heights are used in a series of incremental dynamic analyses. The piers are analysed under the original pulse-like near-field ground motions, their extracted pulse ground motions, and their corresponding non-pulse ground motions, in which the pulse ground motions are subtracted from the original ground motions. It is found that the effect of the pulse ground motion is pronounced, when the pulse period is in close proximity to the natural period of the pier (linear period prior to rocking). However, when the pulse period is far from the natural period of the pier, the effect of the pulse ground motion is negligible, and the non-pulse ground motion is a good representative of the original ground motion. It is also seen that pulse-like near-field and far-field ground motions generally have similar effects on the response of PPS piers.

**Keywords:** Precast post-tensioned segmental columns; resilience-based design; accelerated bridge construction; incremental dynamic analysis; pulse-like near-field ground motions; seismic performance assessment

## 1. Introduction

The research on the performance of precast post-tensioned segmental (PPS) piers is increasing in order to design a bridge structure with less vulnerability and longer lifespan. PPS piers provides a construction technique that can address the demands of a resilient and sustainable transport infrastructure by providing reduction in the construction cost and maintenance cost of the bridges. Unlike the cast-in-place (CIP) piers, which are integrally constructed and connected to their base, the rocking motion of the PPS piers prevents development of large concrete cracks and the permanent plastic deformations particularly at their base. Further, the post-tensioning tendon causes the PPS pier to return to its original position after lateral seismic ground motions, i.e. displacements are recoverable and resilient. So far, many experimental and numerical studies have been carried out to understand static and dynamic behaviour of the PPS piers.

Some experimental studies examined performance of the PPS piers primarily subject to cyclic and dynamic loadings (Billington & Yoon, 2004;Hassanli, Youssef & Mills, 2017;J. Wang, Z. Wang, Tang, Liu & Zhang, 2018;Z. Wang, J. Wang & Zhu, 2018; Yang, Okumus & Ren, 2019; Tong, Zhuo, Jiang, Lei & Liu, 2019). For example, Hewes (2002) studied the behaviour of the PPS piers throughout a number of cyclic tests. The PPS piers were found to have sufficient strength and low energy dissipation capability. Different strategies were proposed to enhance the damping of the PPS piers through cyclic experimental programmes (Z. Wang, J. Wang, & Zhu, 2018; Ou, Chiewanichakorn, Aref & Lee 2007; Chou & Chen, 2006; Marriott, Pampanin & Palermo, 2009;Elgawady & Sha'Lan, 2011). In some studies, real ground motions were used throughout shake table testing to study the dynamic behaviour of the PPS piers with additional

parts for energy dissipation. Motaref, Saiidi and Sanders (2010) tested precast concrete segmental column models with built-in elastomer pads, while Sideris, Aref and Filiatrault (2014), and Sideris, Aref and Filiatrault (2015) introduced a novel PPS pier equipped with hybrid sliding-rocking joints. The use of other dissipators was also tested such as rubber pads (Kashani & Gonzalez-Buelga, 2017;Kashani, Gonzalez-Buelga, Thayalan, Thomas & Alexander 2018) or entangled wire materials (Kashani, Ahmadi, Gonzalez-Buelgai, Zhang & Scarpa, 2019;Ahmadi & Kashani 2019).

Many numerical studies were also conducted on the PPS piers. Detailed finite element (FE) models and fibre-based FE models (Ou, Chiewanichakorn, Aref & Lee, 2007; Zhang & Hao 2019; Dawood, Elgawady, & Hewes, 2012;Do, Pham & Hao, 2018; ElGawady & Dawood, 2012; Motaref, 2011; El Zareef & Schlaich, 2010; Li, Zhao, Alam, Cheng & Wang, 2020) were developed to study the performance of the PPS piers. Simplified analytical models (Ou et al., 2007; Chou & Chen 2006) were also constructed to estimate cyclic performance of the PPS piers. Cai, Zhou and Wang (2019) investigated remaining displacements of the PPS piers with energy-dissipating attachments. In a recent research, Ahmadi and Kashani (2020) created a computationally efficient and experimentally validated FE model for the PPS piers in OpenSees programme (McKenna 2011), where the segments were modelled as elastic blocks and the contact surfaces were simulated using a number of zero-tension elastic springs. The finite element model developed by Ahmadi and Kashani (2021) was used for dynamic analysis of PPS piers subjected to far-fault ground motions, in which performance limit states were defined for the PPS piers. Wang and Guo (2017) focused on the seismic performance of the self-centering prestressed concrete bridge piers with external aluminium dissipators, and a collapse prevention parameter was selected as performance level to evaluate the fragility curves under far-field ground motions. Dawood and ElGawady (2013) used a collapse prevention limit; i.e. the maximum drift of the pier. However, different limit states were not defined for different

performance levels of the piers, which emphasises the need for further research in the definition of more detailed performance limit states and respective fragility curves for PPS piers, particularly under pulse-like ground motions.

On the other hand, pulse-like characteristics of ground motions in proximity of active faults make them completely different from ordinary far-field ground motions. Pulse-like ground motions were found to have detrimental effects on various structures. Many research were devoted to extract pulse component of pulse-like ground motions (Mavroeidis & Papageorgiou, 2002; Mavroeidis & Papageorgiou, 2003; Mavroeidis, Dong & Papageorgiou, 2004; Baker, 2007; Hubbard & Mavroeidis, 2011). Sehhati, Rodriguez-Marek, ElGawady and Cofer (2011) investigated the response of multi-story structures to near-fault ground motions through Incremental Dynamic Analysis (IDA) and simplified pulses are also used to examine their effects on structural response. Kalkan and Kunnath (2006) studied the effects of near-fault ground motions and idealized pulses on the seismic response of steel moment frames. Alavi and Krawinkler (2004) presented the seismic response of elastic and inelastic frame structures to near fault ground motions with forward directivity. In series of different studies, Khoshnoudian and Ahmadi (2013), and Khoshnoudian, Ahmadi and Sohrabi (2014) adopted near-fault ground motions to examine the effects of near-fault records on the seismic response of nonlinear MDOF and soil-MDOF structural systems.

Particularly, in Kalkan and Kunnath' s work (2006), simple pulse models were used to study the effects of pulse period, and it is clearly stated that demands are clearly amplified as the pulse period approaches the fundamental period of the building. However, it is mentioned that simple waveforms do not contain all the characteristics of the actual near-fault ground motions. In a different work, Markis (2014) studied seismic response of free-standing (not post-tensioned) rocking columns using the symmetric Ricker wavelet, defined by pulse period and

amplitude. In both studies, the actual ground motions, their pulse and non-pulse components were not compared to understand the significance of pulse and non-pulse components.

To sum up, although seismic behaviour of the PPS piers has been investigated so far, their performance subject to pulse-like near-field ground motions and their constituent components (pulse- and non-pulse components) yet to be studied. Therefore, the aim of this research is to explore and investigate seismic performance of the PPS piers subject to pulse-like near-field ground motions using an advanced nonlinear finite element model and IDA tool (Vamvatsikos & Allin Cornell, 2002). To this end, an experimentally validated and computationally efficient numerical model in OpenSees programme (McKenna 2011) is used to analyse three PPS piers of different heights. The height of the PPS piers is varied to understand and demonstrate the effects of pulse period on the dynamic response of the PPS piers. Then, IDA curves of the PPS piers and fragility curves are generated subject to 44 far-field ground motions, 40 pulse-like near-field ground motions as well as their pulse and non-pulse ground motion counterparts. Furthermore, the IDA curves are generated and demonstrated individually for selected ground motions from the 40 pulse-like near-field ground motions (pulse-like ground motions with low and long pulse periods) to further understand the effect of pulse components on each PPS pier. The IDA curves and fragility curves of the PPS piers generated from the near-field ground motions are also compared with the far-field ground motions to demonstrate the effects of pulse-like near-field ground motions on the piers. The results of this study indicate the significance of natural periods (linear period prior to rocking) of PPS piers on their response to pulse-like ground motions.

## 2. The Proposed PPS Piers

Performance of three PPS piers with various aspect ratios are studied in this research. As illustrated in Figure 1, the PPS piers are composed of a number of segments, $n$, of width $B$, where the total height of the piers is denoted by $H$. The axial load from the bridge deck is

described as a fraction of the axial capacity of the concrete section, $N/(f_cA_g)$, where $N$ is the axial load, $f_c$ and $A_g$ are the concrete compressive strength and the total cross section area of each pier, respectively. The segments are stabilised by a stainless-steel tendon, which is attached to the base and to the top of the pier. The tendon creates a self-centring property and returns the piers to their initial state after any lateral loading.

Table 1 illustrates the piers and their properties used in this research. The piers are 1, 2, and 4 m high, and are composed of 2, 4, and 8 square segments. The post-tensioning tendon ratios, $\rho = A_t/A_g$ (tendon-to-segment area ratio), of 0.005, 0.01, and 0.02 are selected respectively for the 2, 4, and 8-segment piers such that all piers have the same stiffness for the tendon, $E_tA_t/H$. $E_t$ and $A_t$ are the elastic modulus and area of the tendon respectively. Constant axial load ratio, $N/(f_cA_g) = 0.2$, and initial post-tensioning-to-yield stress ratio, $\sigma_0^t/\sigma_y = 0.4$, are selected for the tendon of the piers.

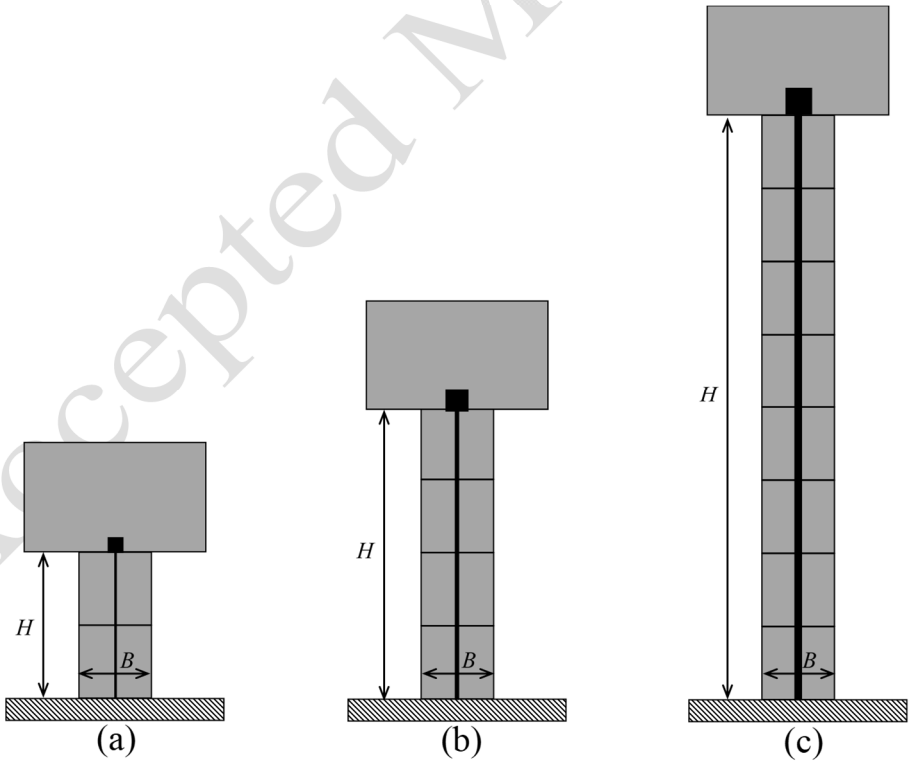


Figure 1. Schematic view of the PPS piers used in this study: (a) 2 segments, C2 (b) 4 segments, C4, and (c) 8 segments, C8.

Table 1. Details of the PPS piers used in this study.

| Column Label. | $n$ (number of segments) | $H$ (m) | $B$ (m) | $\rho$ | $N/(f_cA_g)$ | $\sigma_0^t/\sigma_y$ |
|---|---|---|---|---|---|---|

| | | | | | | |
|---|---|---|---|---|---|---|
| C2 | 2 | 1 | 0.5 | 0.005 | 0.2 | 0.4 |
| C4 | 4 | 2 | 0.5 | 0.01 | 0.2 | 0.4 |
| C8 | 8 | 4 | 0.5 | 0.02 | 0.2 | 0.4 |

To simulate nonlinear seismic behaviour of the PPS piers subject to a ground motion, a 2D Finite Element model developed in OpenSees programme is used (see Figure 2). As shown in Figure 2b, the segments are modelled using Elastic Beam-Column elements, and the post-tensioning stainless steel tendon is modelled with a Truss Element. An Elastic Perfectly Plastic material is used to model the tendon, and an initial tensile strain is included in the Elastic Perfectly Plastic material model to consider the post-tensioning effect of the tendon.

The axial force of the top deck is exerted to the highest node of the piers. Moreover, lump horizontal and vertical masses at the highest node of the piers are used to account for inertial effects of the deck. The Lobatto Quadrature method introduced by Spieth et al. (2004) is adopted to spread the vertical stiffness of the segments over the compression zones at the contact surfaces between the segments (Ahmadi & Kashani 2020). Each compression zone (see Figure 2a) is modelled as a set of axial zero-length spring elements. An elastic zero-tension uniaxial material model is assigned to the joints, which can simulate the joint openings and compression forces at the contact surfaces. Further details on the FE model used and its experimental validation are found in (Ahmadi & Kashani 2020).

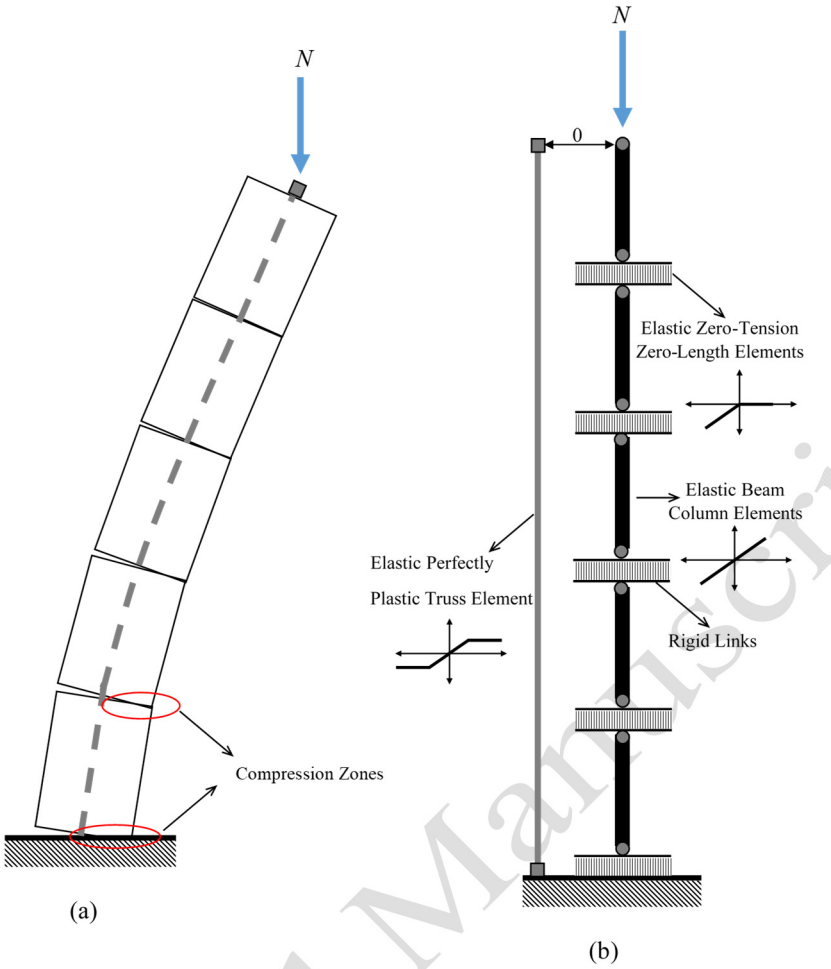


Figure 2. 2D FE modelling of the PPS piers in OpenSees programme.

## 3. The Pulse-like Near-field Ground Motions

The pulse-like ground motion set used herein consists of 40 ground motions. These ground motions contain forward-directivity velocity pulses of varying periods in their strike-normal components, as determined using the methods described by Baker (2007). The pulse periods of the selected ground motions along with other information are summarized in Table 2.

Table 2. Pulse-like near-field ground motion set used in this study (Baker 2007).

| Record number | Earthquake Name | Year | Station Name | Magnitude | Pulse Period (s) |
|---|---|---|---|---|---|
| 1 | Imperial Valley-06 | 1979 | EC County Center FF | 6.53 | 4.51 |
| 2 | Imperial Valley-06 | 1979 | EC Meloland Overpass FF | 6.53 | 3.35 |
| 3 | Imperial Valley-06 | 1979 | El Centro Array #4 | 6.53 | 4.61 |
| 4 | Imperial Valley-06 | 1979 | El Centro Array #5 | 6.53 | 4.05 |
| 5 | Imperial Valley-06 | 1979 | El Centro Array #6 | 6.53 | 3.84 |
| 6 | Imperial Valley-06 | 1979 | El Centro Array #7 | 6.53 | 4.23 |
| 7 | Imperial Valley-06 | 1979 | El Centro Array #8 | 6.53 | 5.39 |
| 8 | Imperial Valley-06 | 1979 | El Centro Differential Array | 6.53 | 5.86 |
| 9 | Morgan Hill | 1984 | Coyote Lake Dam (SW Abut) | 6.19 | 0.95 |

| | | | | | |
|---|---|---|---|---|---|
| 10 | Loma Prieta | 1989 | Gilroy - Gavilan Coll. | 6.93 | 1.79 |
| 11 | Loma Prieta | 1989 | LGPC | 6.93 | 4.39 |
| 12 | Landers | 1992 | Lucerne | 7.28 | 5.10 |
| 13 | Landers | 1992 | Yermo Fire Station | 7.28 | 7.50 |
| 14 | Northridge-01 | 1994 | Jensen Filter Plant | 6.69 | 3.53 |
| 15 | Northridge-01 | 1994 | Jensen Filter Plant Generator | 6.69 | 3.53 |
| 16 | Northridge-01 | 1994 | Newhall - Fire Sta | 6.69 | 1.04 |
| 17 | Northridge-01 | 1994 | Newhall - W Pico Canyon Rd. | 6.69 | 2.41 |
| 18 | Northridge-01 | 1994 | Rinaldi Receiving Sta | 6.69 | 1.23 |
| 19 | Northridge-01 | 1994 | Sylmar - Converter Sta | 6.69 | 3.48 |
| 20 | Northridge-01 | 1994 | Sylmar - Converter Sta East | 6.69 | 3.53 |
| 21 | Northridge-01 | 1994 | Sylmar - Olive View Med FF | 6.69 | 3.11 |
| 22 | Kobe, Japan | 1995 | KJMA | 6.90 | 0.95 |
| 23 | Kobe, Japan | 1995 | Takarazuka | 6.90 | 1.43 |
| 24 | Kocaeli, Turkey | 1999 | Gebze | 7.51 | 5.79 |
| 25 | Chi-Chi, Taiwan | 1999 | CHY028 | 7.62 | 2.24 |
| 26 | Chi-Chi, Taiwan | 1999 | CHY101 | 7.62 | 4.59 |
| 27 | Chi-Chi, Taiwan | 1999 | TCU049 | 7.62 | 11.65 |
| 28 | Chi-Chi, Taiwan | 1999 | TCU052 | 7.62 | 8.36 |
| 29 | Chi-Chi, Taiwan | 1999 | TCU053 | 7.62 | 12.84 |
| 30 | Chi-Chi, Taiwan | 1999 | TCU054 | 7.62 | 10.47 |
| 31 | Chi-Chi, Taiwan | 1999 | TCU068 | 7.62 | 12.17 |
| 32 | Chi-Chi, Taiwan | 1999 | TCU075 | 7.62 | 5.18 |
| 33 | Chi-Chi, Taiwan | 1999 | TCU076 | 7.62 | 3.98 |
| 34 | Chi-Chi, Taiwan | 1999 | TCU082 | 7.62 | 8.98 |
| 35 | Chi-Chi, Taiwan | 1999 | TCU087 | 7.62 | 9.37 |
| 36 | Chi-Chi, Taiwan | 1999 | TCU101 | 7.62 | 10.04 |
| 37 | Chi-Chi, Taiwan | 1999 | TCU102 | 7.62 | 9.74 |
| 38 | Chi-Chi, Taiwan | 1999 | TCU103 | 7.62 | 8.24 |
| 39 | Chi-Chi, Taiwan | 1999 | TCU122 | 7.62 | 10.88 |
| 40 | Chi-Chi, Taiwan | 1999 | WGK | 7.62 | 4.39 |

One benefit of the technique used by Baker (2007) for the identification of the pulses is to extract the pulse portion from the original ground motion (OGM), which is here named as pulse ground motion (PGM). The subtraction of the PGM from the OGM gives the residual portion of the ground motion, which is here called non-pulse ground motion (NPGM). Figure 3 shows the acceleration time history of the original ground motion for record no. 30 as well as its counterparts. Additionally, an ensemble of 44 far-field ground motions is adopted in the analysis of the piers to be compared with the results of the pulse-like near-field ground motions. The 44 far-field ensemble is given in FEMA P659 (2009), and contains 22 pairs of horizontal

ground motions with two components from sites located within a distance greater than 10 km from fault rupture.

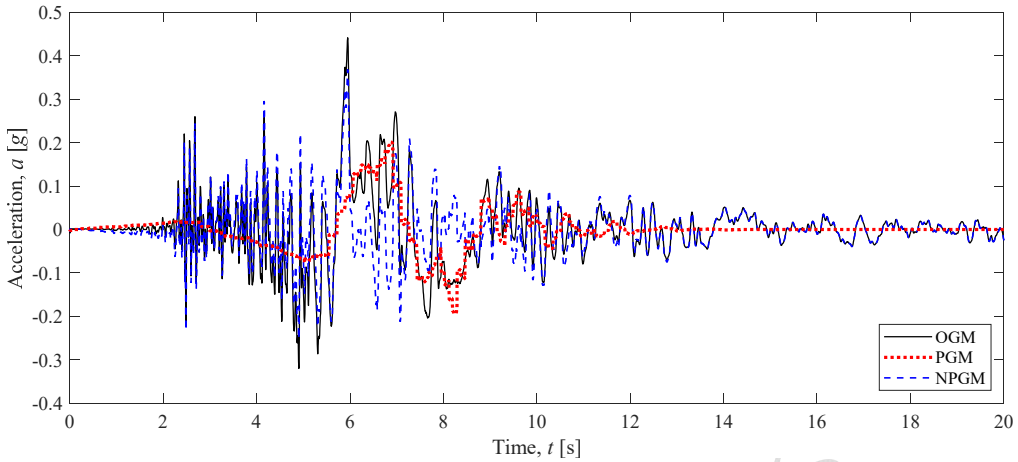


Figure 3. Acceleration time histories of record no. 30: original ground motion (OGM), pulse ground motion (PGM), and non-pulse ground motion (NPGM).

## 4. Analyses, Results, and Discussion

This section presents and discusses the results of IDA analysis and fragility curves for the referred PPS piers (Section 2) subjected to ground motions given in Section 3. ID analysis determines seismic performance of the structure subject to a series of ground motions with various levels of intensities. First, IDA results are presented for the comparison between far-field and original near-field ground motion records (pulse-like ground motions). Following this, to investigate the effects of the pulse components of the near-field ground motions further, the median IDA curves of the original, pulse and non-pulse ground motions are compared. Finally, fragility curves are obtained for each ground motion.

### 4.1 Incremental Dynamic Analysis (IDA) and Results of OGM and Far-Field Ground Motions

The intensity measure (IM) selected for the IDA analysis in this study is the 5% damped spectral acceleration response of the original ground motions at the pier's first mode period, $S_a$ ($T_1$, 5%). $T_1$ is the first natural vibration period of the pier at very low-amplitude dynamic excitations where the joints are still close, and no rocking motion has initiated. This period is

determined using eigenvalue analysis of the piers. The first natural periods of the C2, C4, and C8 piers are 0.09s, 0.26s, and 0.75s respectively. The higher the pier becomes the longer its natural period is. It should be noted that the natural periods of these piers comply with the existing ordinary bridge piers (Ahmadi & Kashani 2020). Prior to the IDA of each pier, the original ground motions are first scaled to 1 at the natural period of each pier using their 5% damped spectra. These scale factors are also used to scale the PGM and NPGM sets of the original near-field ground motions, i.e. OGMs. The IM is then changed from 0.05g to 1g with the increment of 0.05g. Small IM value of 0.005g very close to 0 is also considered to ensure elastic behaviour of the piers before their rocking initiation.

Figures 4, 5, and 6 show median IDA curves of top drift, base rotation, normalised base shear, and normalised base moment of the piers. The top drift, $\Delta/H$, is defined as the displacement of the tip of the pier, $\Delta$, normalised by the total height of the pier, $H$. The base shear, $V$, is normalised by the total weight of the pier including the segments and the top mass, $W$. The median IDA curves of the far-field ground motions follow a close trend as the median IDA curves of the pulse-like near-field ground motions, as shown in Figures 4, 5, and 6. Thus, the pulse effects on general response of the piers are insignificant. Figure 7 shows median IDA curves of normalised post-tensioning force of the far-field and original near-field ground motion records (pulse-like ground motions). The tendon force ratio in Figure 7 at zero spectral acceleration is less than 0.4. This drop in the tendon force is because of the post-tensioning loss due to elastic shortening of the segments as well as the flexibility of rocking surfaces under gravity loads. This post-tensioning loss is higher for the slender piers as they have more number of segments and joints. Similar to the general response results in Figures 4, 5 and 6, the difference between the median IDA curves of the far-field and the pulse-like near-field ground motions is insignificant. This implies the negligible effect of the near-field pulses on the post-tensioning force of the piers.

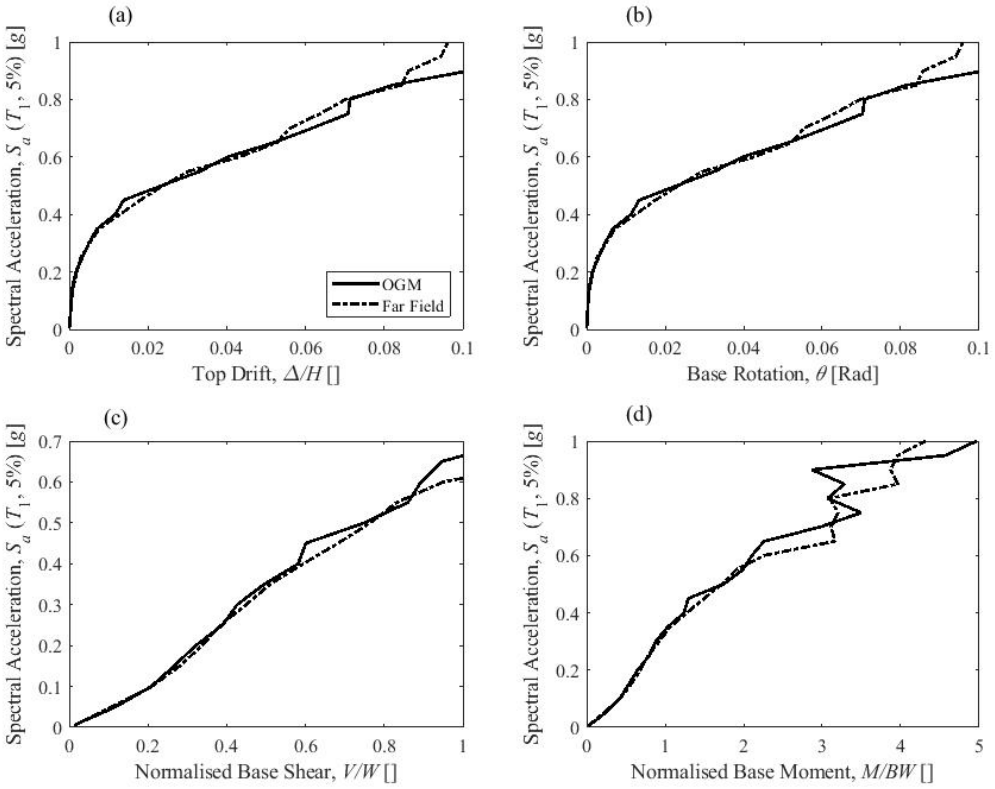


Figure 4. Median IDA curves for the pier C2: (a) top drift, (b) base rotation, (c) normalised base shear, and (d) normalised base moment.

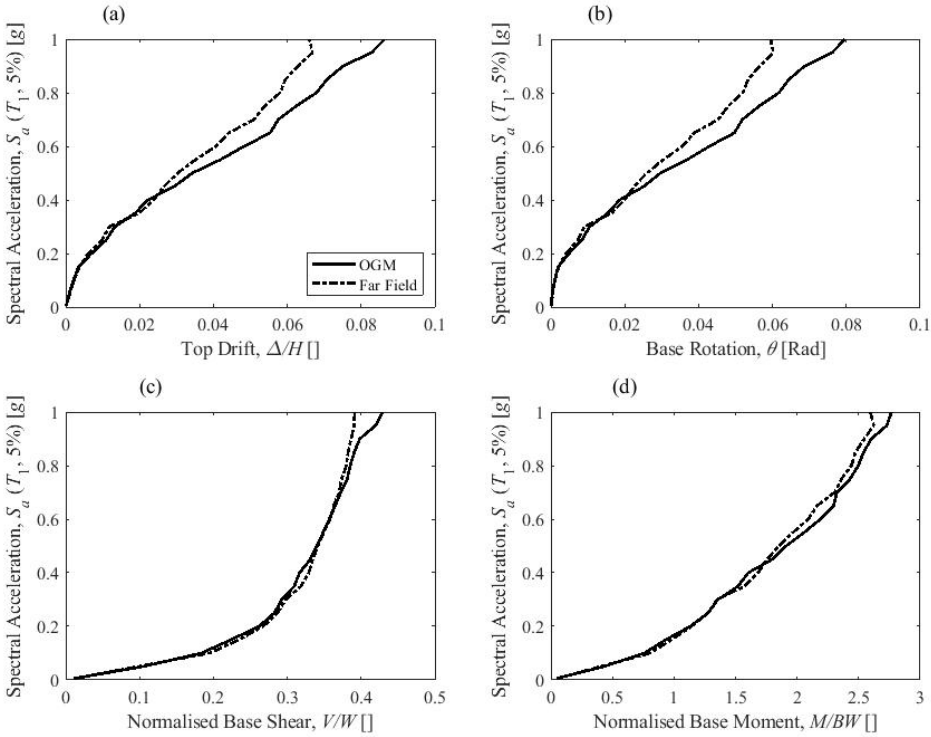


Figure 5. Median IDA curves for the pier C4: (a) top drift, (b) base rotation, (c) normalised base shear, and (d) normalised base moment.

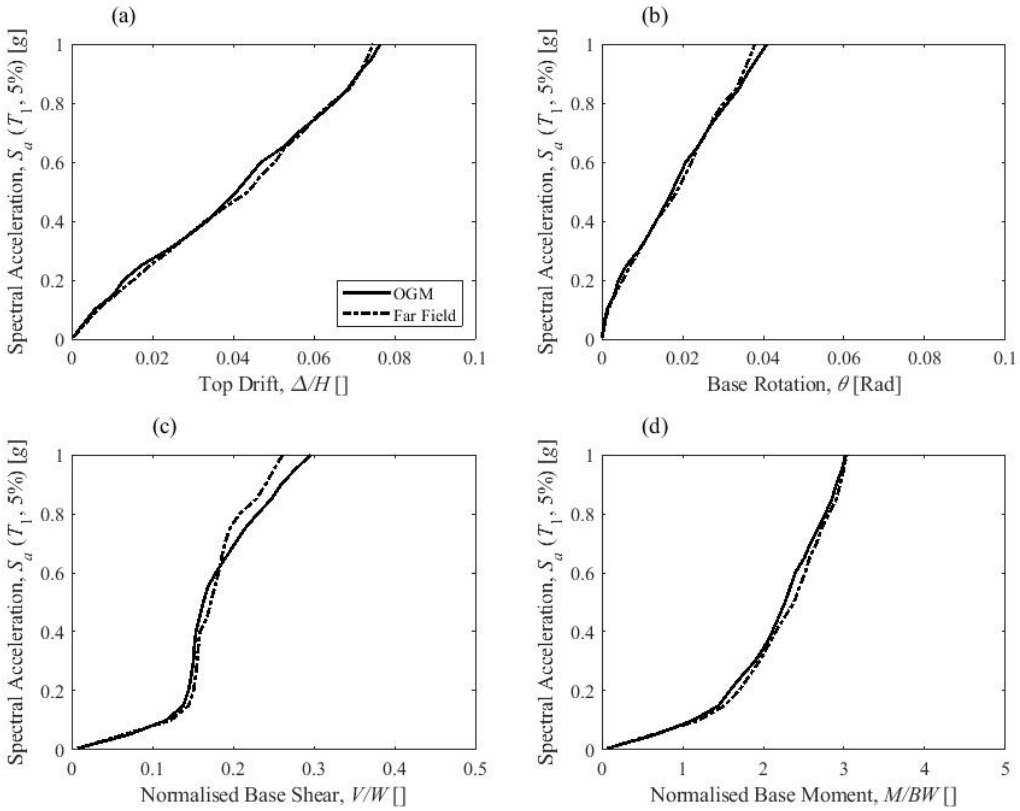


Figure 6. Median IDA curves for the pier C8: (a) top drift, (b) base rotation, (c) normalised base shear, and (d) normalised base moment.

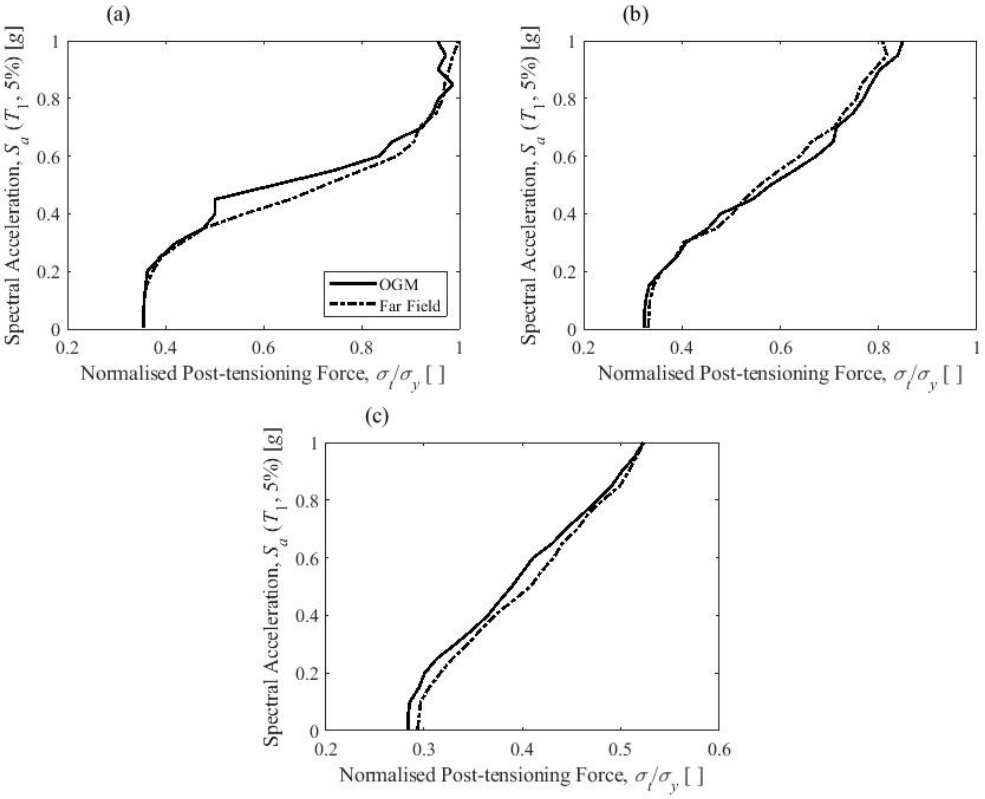


Figure 7. Median IDA curves of normalised post-tensioning force of the tendon for: (a) C2, (b) C4, and (c) C8.

### 4.2 Incremental Dynamic Analysis (IDA) and Results of PGM

To examine the effects of the pulse components of the near-field ground motions further, the median IDA curves of the original, pulse and non-pulse ground motions are compared. Figures 8, 9, and 10 show the median IDA curves of top drift, base rotation, normalised base shear, and normalised base moment of the piers. The median responses of the PGMs are much smaller than those of the NPGMs, as shown in Figures 8, 9, and 10. Further, the median responses of the NPGMs are very close to those of the OGMs, which shows less significant effects of the PGMs on the median response of the piers.

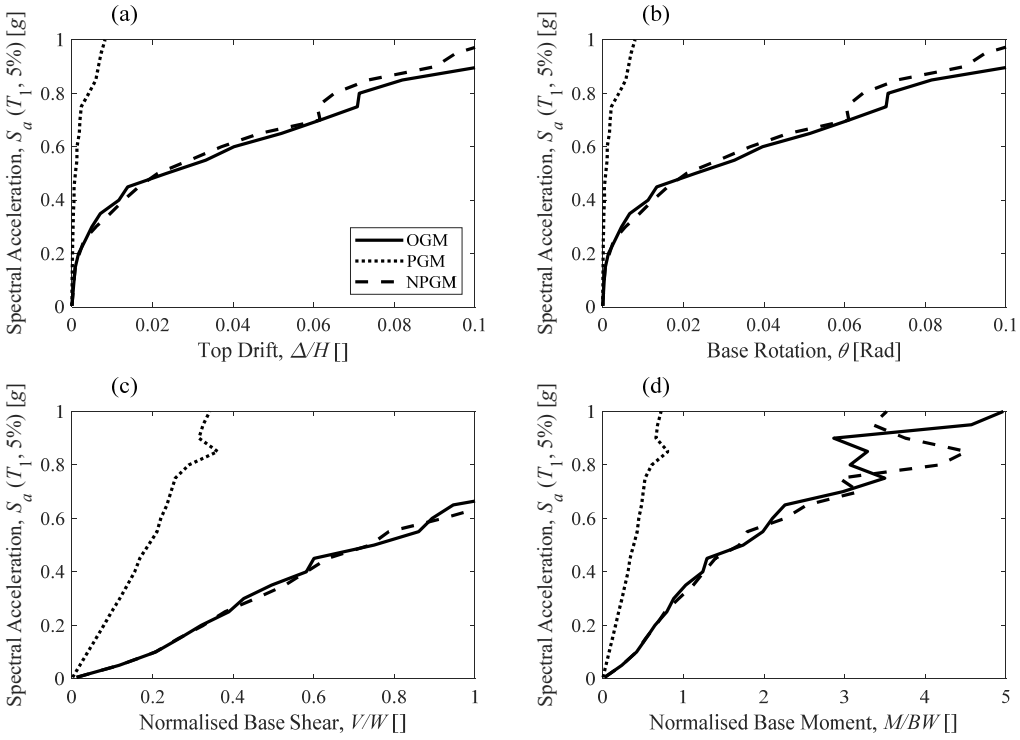


Figure 8. Median IDA curves for the pier C2: (a) top drift, (b) base rotation, (c) normalised base shear, and (d) normalised base moment.

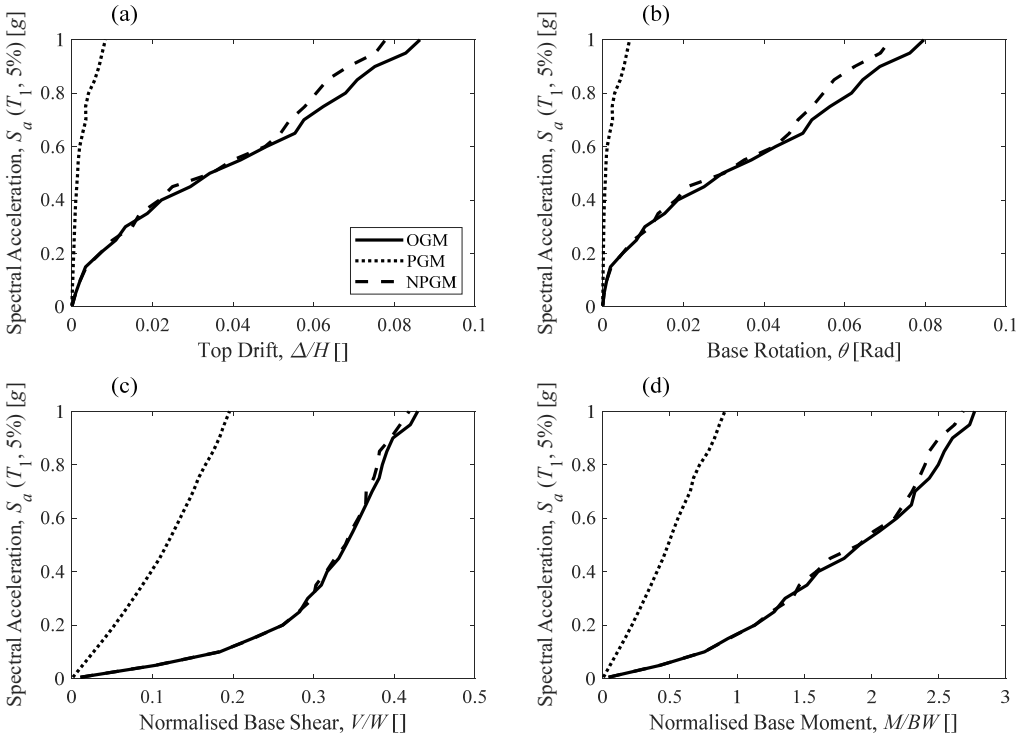


Figure 9. Median IDA curves for the pier C4: (a) top drift, (b) base rotation, (c) normalised base shear, and (d) normalised base moment.

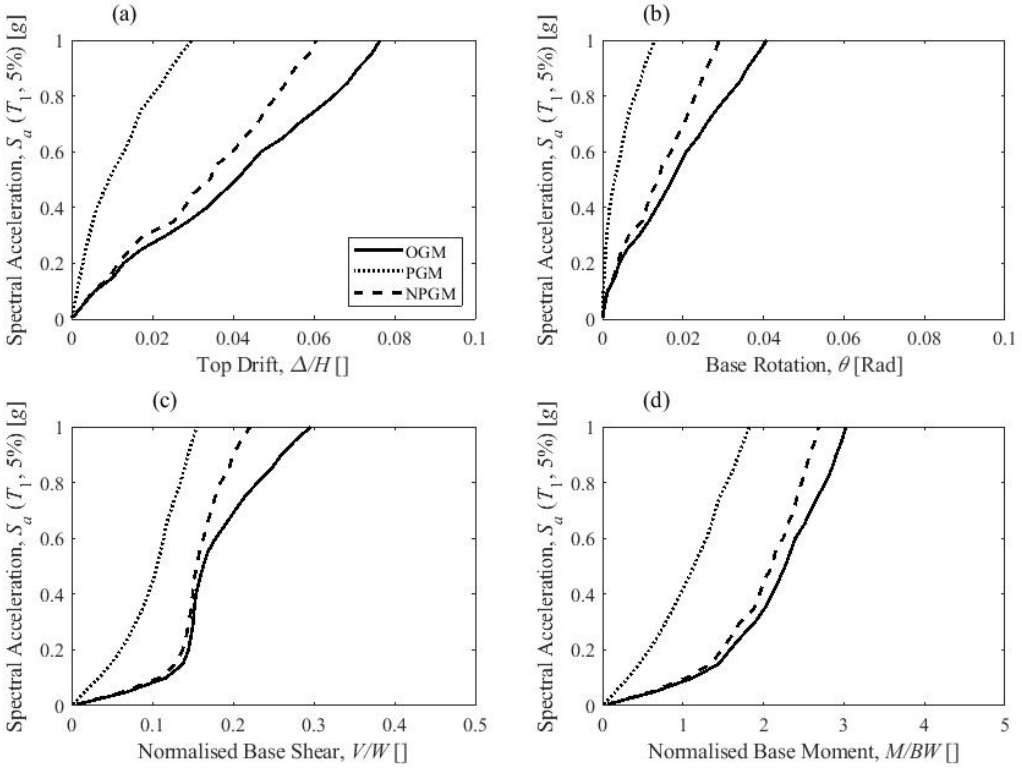


Figure 10. Median IDA curves for the pier C8: (a) top drift, (b) base rotation, (c) normalised base shear, and (d) normalised base moment.

Figure 11 shows the median IDA curves of the normalised post-tensioning force for the OGM, PGM and NPGM records. As clearly seen, the pulse effects are very insignificant, and ignoring the pulse component of the OGMs slightly affects the post-tensioning force of the tendon. Nearly vertical median IDA curves of the PGMs at low IM value show that the piers are not generally excited by the PGMs, and hence, the piers do not have any lateral motion at small IM values. However, at high IM values, slight increase in the tendon force ratio shows that the piers experience slight rocking.

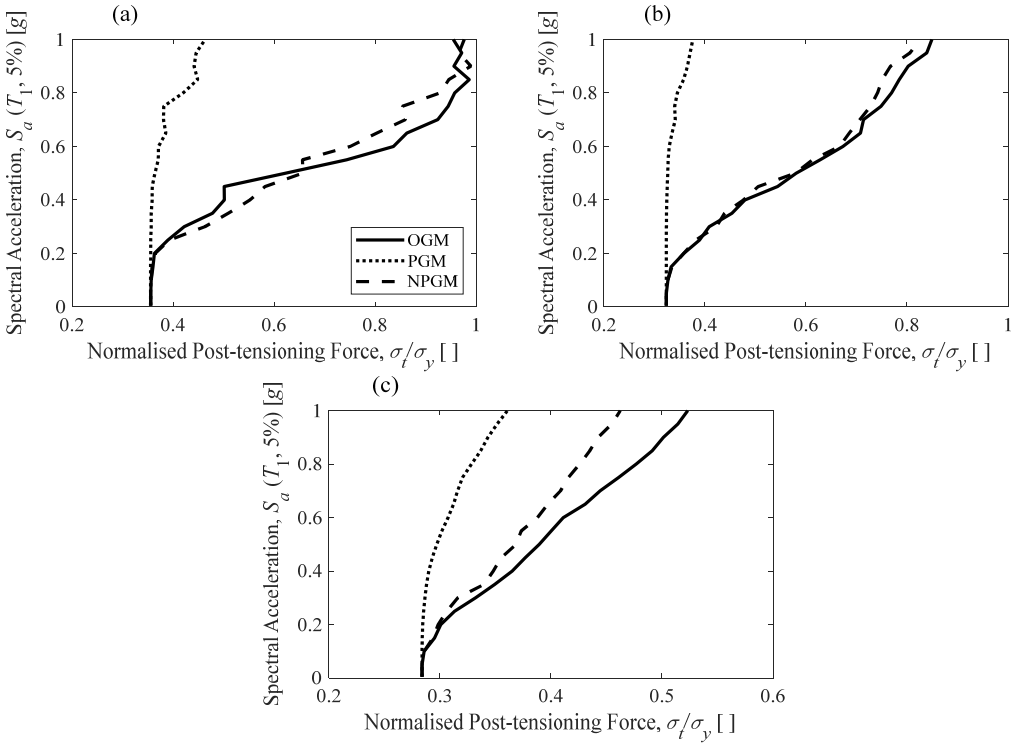


Figure 11. Median IDA curves of normalised post-tensioning force of the tendon for: (a) C2, (b) C4, and (c) C8.

The median IDA curves of all ground motions demonstrate the general effect of the pulse component on the response of the piers. Thus, the responses of the piers to pulse-like ground motions will be individually scrutinised to investigate the effects of the pulse period. To show the effects of the pulse period, the results of some exemplary pulse-like ground motions with short and long pulse periods are presented. Figures 12, 13, and 14 show IDA curves of the piers

C2, C4, and C8 for top drift, base rotation, normalised base shear, and normalised base moment subject to record no. 9 with extracted pulse period of 0.952s. This record has the lowest pulse period among all 40 pulse-like near-field ground motions. As seen in Figures 12 and 13, the effect of the PGM on the piers C2 and C4 is very small compared to NPGM and OGM, which is well justified by the fact that the first natural period of the piers falls far below the pulse period of the PGM. Thus, none of the modes of the piers C2 and C4 is excited by the PGM. However, the NPGM well represents the OGM at IM values below 0.4 for the pier C2 and 0.8 for the pier C4. For higher IM values, the NPGM's results are very different to those of the OGM as the nonlinear behaviour of the pier is dominant. As shown in (Ahmadi and Kashani 2020), the frequency response functions of PPS piers exhibit a dynamic softening, where the system's stiffness drops as the excitation amplitude increases. Thus, at higher IM values, the first period of the pier significantly elongates. This means that the presence of the PGM can excite the nonlinear modes of the piers at higher IM values. The effects of the PGM and NPGM become different for the pier C8. As seen in Figure 14, the effect of the PGM is far greater than the NPGM. In this case, the effect of the OGM is well presented by a single pulse motion, PGM. This is because of the fact that the period of the pier C8, 0.75s, is close enough to the pulse period, 0.95s, so that the first mode of the pier is excited by the PGM.

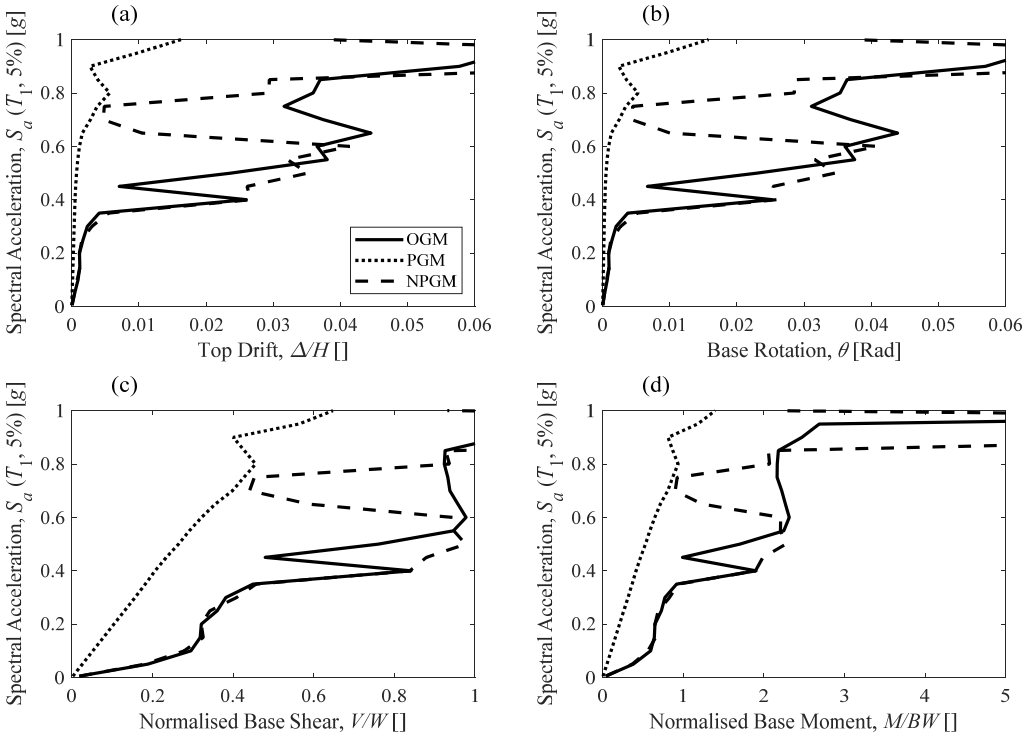


Figure 12. IDA curves of record no. 9 for the pier C2: (a) top drift, (b) base rotation, (c) normalised base shear, and (d) normalised base moment

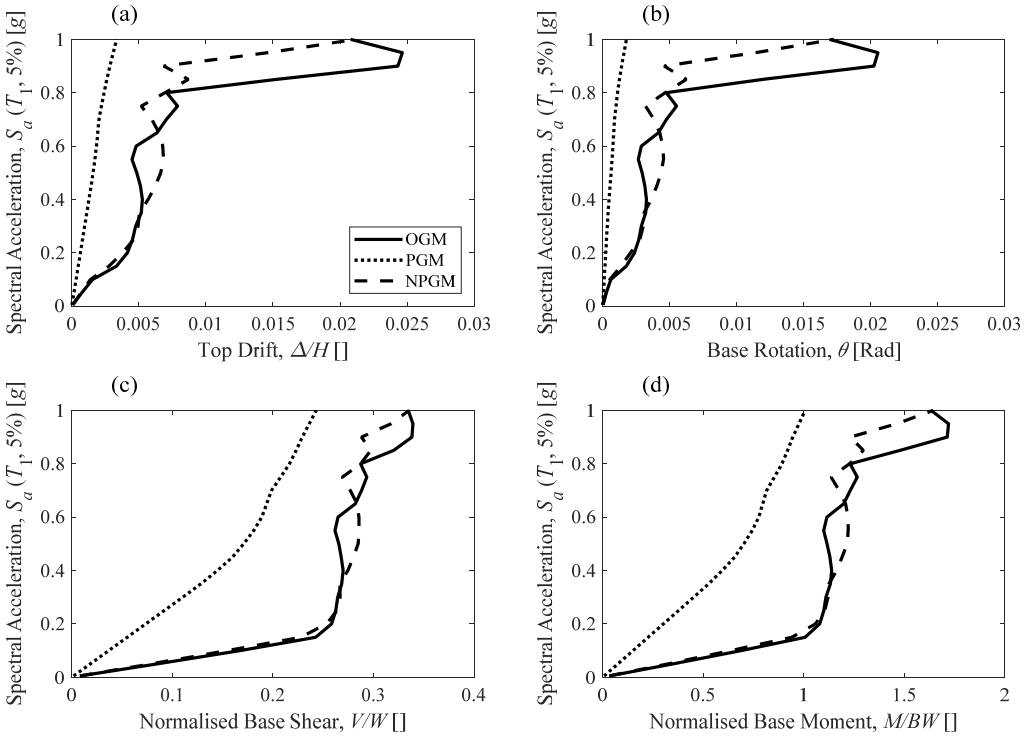


Figure 13. IDA curves of record no. 9 for the pier C4: (a) top drift, (b) base rotation, (c) normalised base shear, and (d) normalised base moment.

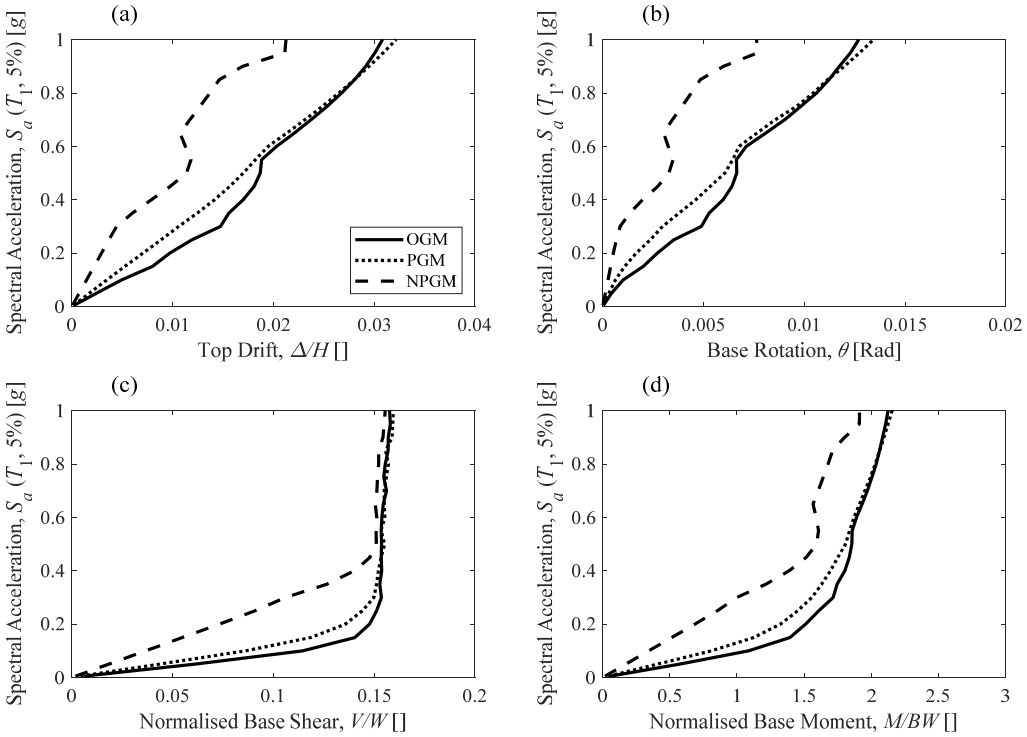


Figure 14. IDA curves of record no. 9 for the pier C8: (a) top drift, (b) base rotation, (c) normalised base shear, and (d) normalised base moment.

Figure 15 shows IDA curves of the pier C8 for top drift, base rotation, normalised base shear, and normalised base moment subject to record no. 30 with very long pulse period of 10.47s. In this case, the pulse period is far higher than the first natural period of the pier, and hence, the effect of the PGM is negligible. Further, the NPGM well represents the responses of the pier subject to the OGM, and exclusion of the pulse component does not influence the responses significantly. The results of the pier C2 and C4 subject to record no. 30 are not presented, since their results exhibited the same trend as those for the pier C8.

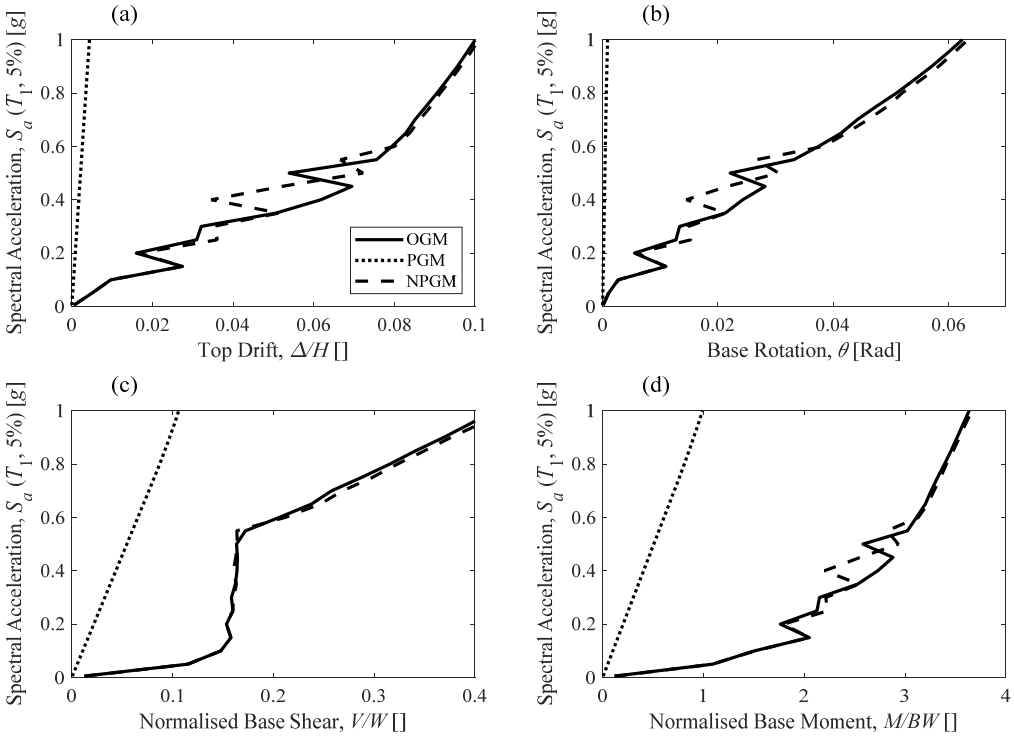


Figure 15. IDA curves of record no. 30 for the pier C8: (a) top drift, (b) base rotation, (c) normalised base shear, and (d) normalised base moment.

### 4.3 Fragility Curves

The fragility curves for the piers C2, C4, and C8 are developed based on the IDA results presented in Section 4.1. The seismic fragility function is commonly defined as a standard lognormal cumulative distribution function:

$$P\left(DS \geq ds \mid IM = x\right) = \phi\left(\frac{\ln\left(x\right) - \ln\left(\theta\right)}{\beta}\right) \tag{1}$$

in which $P\left(DS \geq ds \mid IM = x\right)$ is the conditional probability that a ground motion of $IM = x$ results in a particular damage state equal or greater than $ds$; $\phi$ is the standard lognoraml distribution function; $\theta$ and $\beta$ are the median and logarithmic standard deviation of the fragility function, respectively. The moment estimator method is used to determine $\theta$ and $\beta$:

$$\ln\left(\theta\right) = \frac{1}{N}\sum_{i=1}^{N}\ln\left(IM_i\right) \tag{2}$$

$$\beta = \sqrt{\frac{1}{N-1}\sum_{i=1}^{N}\left(\ln\left(IM_i\right)-\ln\left(\theta\right)\right)^2} \tag{3}$$

in which, $N$ is the number of ground motions used for IDA analysis and $IM_i$ is the IM level at which the damage state starts.

Determination of unique fragility curves requires the identification and definition of the damage limit states for the PPS piers. The important damage states for the PPS piers can be defined in two important states: (1) yielding of the tendons, since the post-tensioned tendon provides global stability and self-centering capability of the PPS piers; and (2) extensive strength drop of the PPS piers due to P-delta effects. Therefore, the stress values of $0.5\sigma_y$, $0.7\sigma_y$, and $0.9\sigma_y$ at which the tendon represents High Stability, Low Stability, and Damage Avoidance states, respectively. In addition, the Damage Avoidance state starts when the strength loss of the piers reaches 20%. The quantative definition of the referred states denotes the behavior of the PPS pier components that are in elastic range in order to avoid damage.

Figure 16 illustrates the pushover analysis results of each pier for the possible failure mechanisms. According to Figure 16, for the pier C2, the tendon reaches the defined stresses of $0.5\sigma_y$, $0.7\sigma_y$, and $0.9\sigma_y$ at the top drift values of 0.01, 0.02, and 0.03 for the states of High Stability, Low Stability, and Damage Avoidance, respectively. Furthermore, the 20% strength loss of the pier C2 occurs at the top drift value of 0.09 (Figure 16a). For the pier C4, the tendon reaches the referred states at the top drifts of 0.025, 0.05, and 0.07 that are equal or less than 0.07, at which the 20% strength loss occurs (Figure 16a). Hence, for the piers C2 and C4, the dominant failure mode is the yielding of the tendon. However, for the pier C8, the 20% strength loss is the dominant failure mode; therefore, the top drift of 0.028, at which the 20% strength loss starts, specifies the Damage Avoidance state.

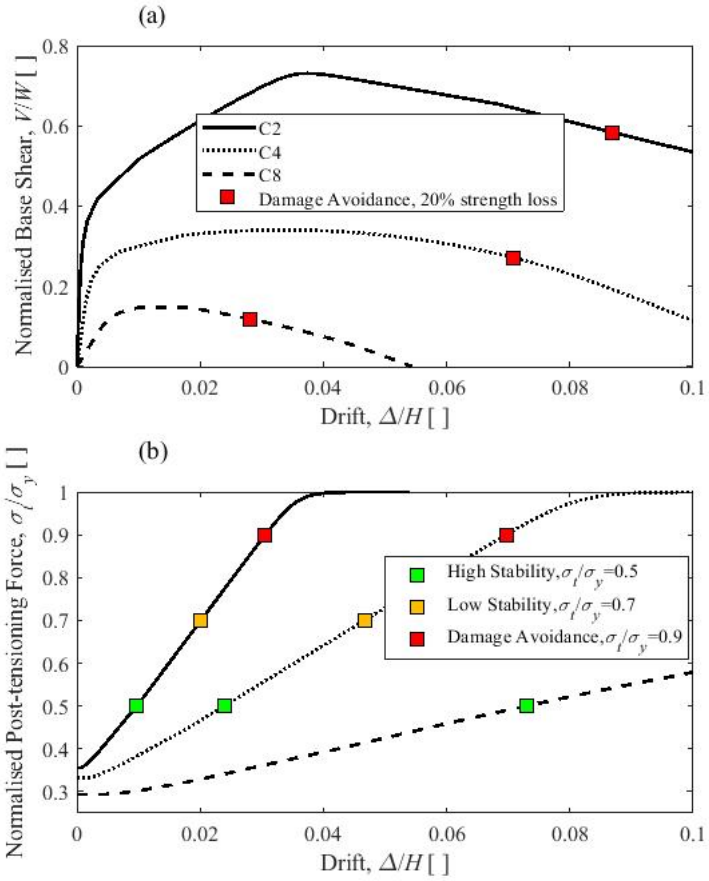


Figure 16. Pushover analysis of the piers: (a) normalised base shear versus drift curves, and (b) normalised post-tensioning force versus top drift curves.

Figure 17 compares the fragility curves of the pier C2 for far-field and pulse-like near-field ground motions. As seen, the fragility curves for both the far-field and near-field ground motions are very similar, which again emphasizes on negligible effect of the pulse component. Figure 18 shows the fragility curves of the OGM, PGM and NPGM for the pier C2. For each state, the OGM and NPGM fragility curves slightly differ. Further, the PGM reaches to probability of exceedance of 0.9 for each defined state at 1.1g.

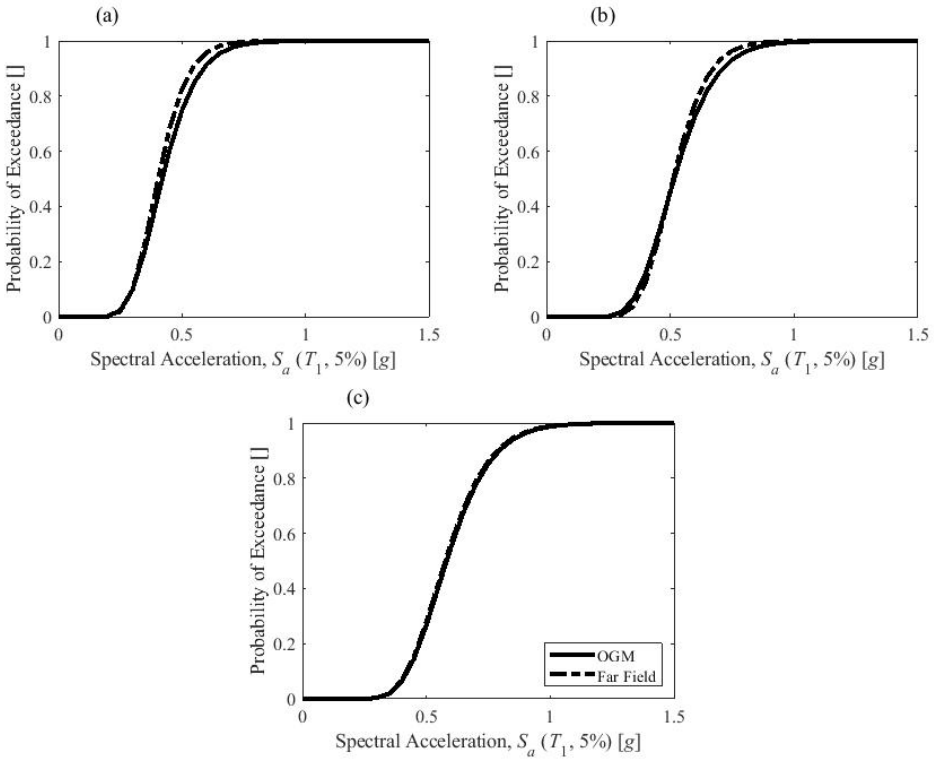


Figure 17. Fragility curves of the piers C2: (a) High Stability, (b) Low Stability, and (c) Damage Avoidance.

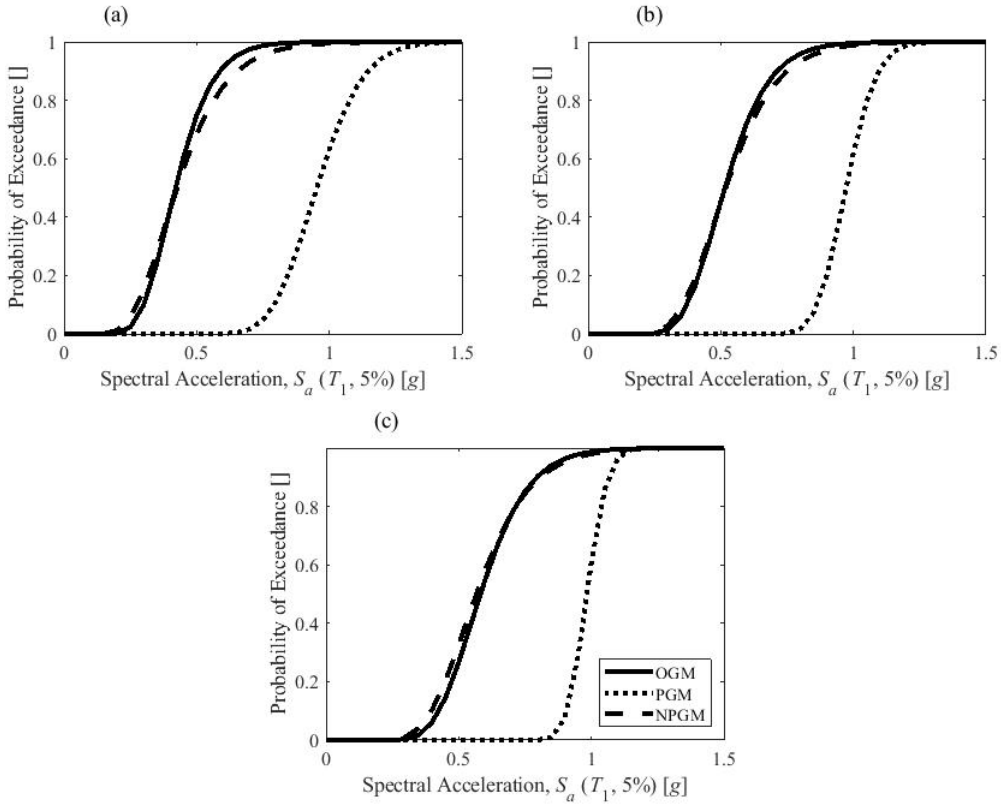


Figure 18. Fragility curves of the pier C2: (a) High Stability, (b) Low Stability, and (c) Damage Avoidance.

Figure 19 compares the fragility curves of the pier C4 for the far-field and pulse-like near-field ground motions, and Figure 20 illustrates the fragility curves of the OGM, PGM and NPGM for the pier C4. Similar to the pier C2, for each fragility curve representation state, the difference in the fragility curves of the OGM and NPGM is very slight, and the PGM reaches to probability of exceedance of 0.9 for each referred state at 1.05g. Finally, Figure 21 shows the fragility curves of the pier C8. The pulse-like near-field ground motions follow a close trend to the far-field ground motions (see Figure 21a), which is similar to the piers C2 and C4. However, as opposed to the piers C2 and C4, the OGM reaches to probability of exceedance of 0.9 at 0.74g. This difference is due to the fact that the pier C8 is the highest pier with the longest natural period.

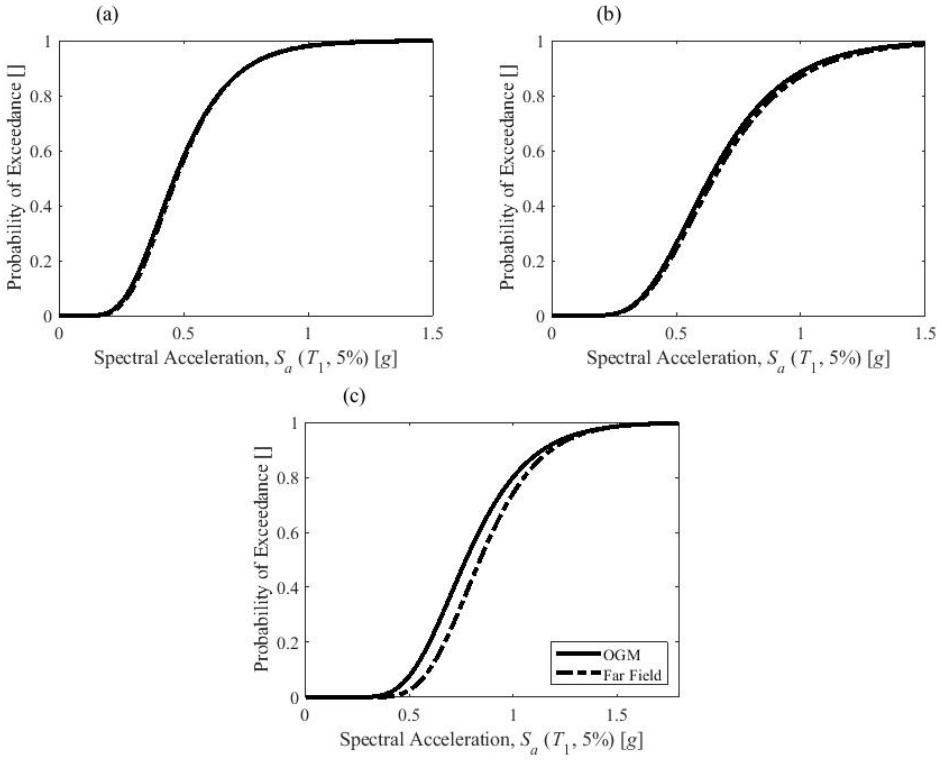


Figure 19. Fragility curves of the pier C4: (a) High Stability, (b) Low Stability, and (c) Damage Avoidance.

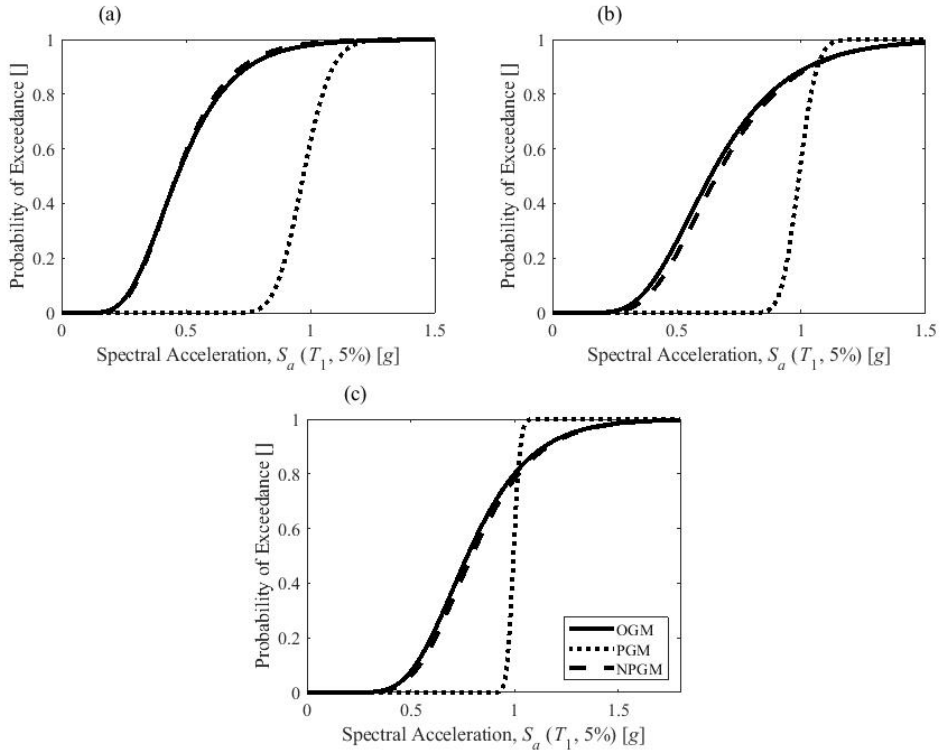


Figure 20. Fragility curves of the pier C4: (a) High Stability, (b) Low Stability, and (c) Damage Avoidance.

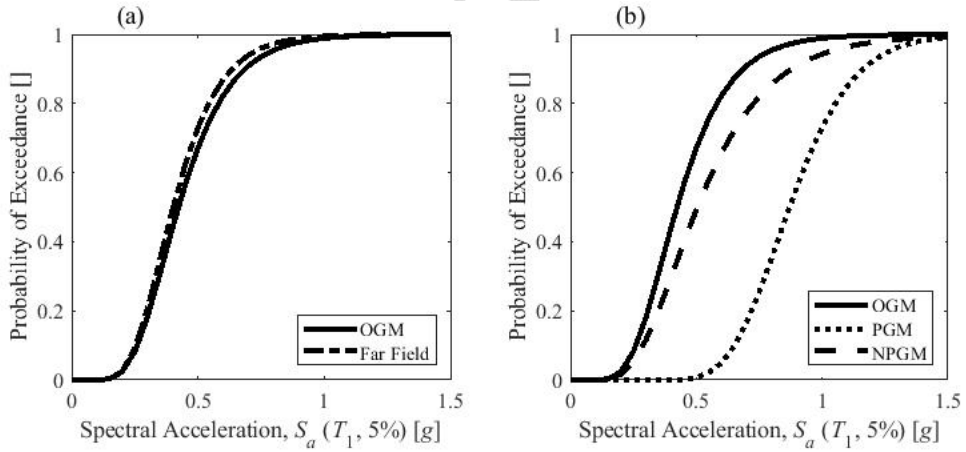


Figure 21. Fragility curves of the piers C8 for Damage Avoidance: (a) far-field and pulse-like near-field ground motions (b) OGM, PGM, and NPGM.

## 5. Conclusions

The PPS piers provides robust, low-maintenance and demountable accelerated bridge construction technique that could be resilient to natural hazards. To expand their application in seismic regions, the current study explores and investigates the effect of pulse-like near-field

ground motions on structural performance of PPS piers using extensive IDAs on three experimentally validated PPS piers. 44 far-field ground motions including 22 pairs of two horizontal components and 40 pulse-like near-field including pulse and non-pulse ground motions are used in the analyses.

The IDA curves of the piers demonstrate that the pulse-to-pier period ratio plays a vital role in the significance of the pulse ground motion. If this ratio is in the vicinity of 1, meaning the pulse period is close to the natural period of the pier, the effect of the pulse ground motion is pronounced, and the effect of the non-pulse ground motion is negligible. Conversely, if the pulse-to-pier period ratio is far from 1, the non-pulse ground motion is dominant, and the effect of the pulse ground motion is insignificant. Furthermore, slight difference in the IDA and fragility curves of the pulse-like near-field and far-field ground motions shows the negligible effect of the pulse component on the response of the piers.

The results of this study suggest that new ground motion decomposition strategies must be developed to include natural periods of structures as an influential factor in identification of effective pulses of near-field ground motions. Thus, perhaps more than a single pulse may need to be considered to reach a good estimation of the effects of near-field ground motions.

## Acknowledgement

The authors acknowledge the support received by the UK Engineering and Physical Sciences Research Council (EPSRC) for a Prosperous Nation [grant number EP/R039178/1]**:** *SPINE: Resilience-Based Design of Biologically Inspired Columns for Next-Generation Accelerated Bridge Construction*].

# References

Ahmadi, E., and M. M. Kashani. 2019. "On the Use of Entangled Wire Materials in Pre-Tensioned Rocking Columns." in *Journal of Physics: Conference Series*. Vol. 1264.

Ahmadi, Ehsan, and Mohammad M. Kashani. 2020. "Numerical Investigation of Nonlinear Static and Dynamic Behaviour of Self-Centring Rocking Segmental Bridge Piers." *Soil Dynamics*

*and Earthquake Engineering* 128(September 2019):105876. doi: 10.1016/j.soildyn.2019.105876.

Ahmadi, Ehsan, and Mohammad M. Kashani. 2021. "Seismic Vulnerability Assessment of Precast Post-Tensioned Segmental Bridge Piers Subject to Far-Fault Ground Motions." *Structures* 34:2566–79. doi: 10.1016/j.istruc.2021.09.041.

Alavi, Babak, and Helmut Krawinkler. 2004. "Behavior of Moment-Resisting Frame Structures Subjected to near-Fault Ground Motions." *Earthquake Engineering and Structural Dynamics*. doi: 10.1002/eqe.369.

Baker, Jack W. 2007a. "Quantitative Classification of Near-Fault Ground Motions Using Wavelet Analysis." *Bulletin of the Seismological Society of America*. doi: 10.1785/0120060255.

Baker, Jack W. 2007b. "Quantitative Classification of Near-Fault Ground Motions Using Wavelet Analysis." *Bulletin of the Seismological Society of America*. doi: 10.1785/0120060255.

Billington, S. L., and J. K. Yoon. 2004. "Cyclic Response of Unbonded Posttensioned Precast Columns with Ductile Fiber-Reinforced Concrete." *Journal of Bridge Engineering*.

Cai, Zhong Kui, Zheng Zhou, and Zhenyu Wang. 2019. "Influencing Factors of Residual Drifts of Precast Segmental Bridge Columns with Energy Dissipation Bars." *Advances in Structural Engineering*. doi: 10.1177/1369433218780545.

Cao, Zhiliang, Hao Wang, and Tong Guo. 2017. "Fragility Analysis of Self-Centering Prestressed Concrete Bridge Pier with External Aluminum Dissipators." *Advances in Structural Engineering* 20(8):1210–22. doi: 10.1177/1369433216673376.

Chou, Chung Che, and Yu Chih Chen. 2006a. "Cyclic Tests of Post-Tensioned Precast CFT Segmental Bridge Columns with Unbonded Strands." *Earthquake Engineering and Structural Dynamics*. doi: 10.1002/eqe.512.

Chou, Chung Che, and Yu Chih Chen. 2006b. "Cyclic Tests of Post-Tensioned Precast CFT Segmental Bridge Columns with Unbonded Strands." *Earthquake Engineering and Structural Dynamics*. doi: 10.1002/eqe.512.

Dawood, Haitham, Mohamed Elgawady, and Joshua Hewes. 2012. "Behavior of Segmental Precast Posttensioned Bridge Piers under Lateral Loads." *Journal of Bridge Engineering*. doi: 10.1061/(ASCE)BE.1943-5592.0000252.

Dawood, Haitham M., and Mohamed ElGawady. 2013. "Performance-Based Seismic Design of Unbonded Precast Post-Tensioned Concrete Filled GFRP Tube Piers." *Composites Part B: Engineering* 44(1):357–67. doi: 10.1016/j.compositesb.2012.04.065.

Do, Tin V., Thong M. Pham, and Hong Hao. 2018. "Numerical Investigation of the Behavior of Precast Concrete Segmental Columns Subjected to Vehicle Collision." *Engineering Structures*. doi: 10.1016/j.engstruct.2017.11.033.

ElGawady, Mohamed A., and Haitham M. Dawood. 2012. "Analysis of Segmental Piers Consisted of Concrete Filled FRP Tubes." *Engineering Structures*. doi: 10.1016/j.engstruct.2012.01.001.

Elgawady, Mohamed A., and Ahmad Sha'Lan. 2011. "Seismic Behavior of Self-Centering Precast Segmental Bridge Bents." *Journal of Bridge Engineering*. doi: 10.1061/(ASCE)BE.1943-5592.0000174.

FEMA P695. 2009. *Quantification of Building Seismic Performance Factors*.

Hassanli, Reza, Osama Youssf, and Julie E. Mills. 2017. "Seismic Performance of Precast Posttensioned Segmental FRP-Confined and Unconfined Crumb Rubber Concrete Columns." *Journal of Composites for Construction*. doi: 10.1061/(ASCE)CC.1943-5614.0000789.

Hubbard, Derek T., and George P. Mavroeidis. 2011. "Damping Coefficients for Near-Fault Ground Motion Response Spectra." *Soil Dynamics and Earthquake Engineering*. doi: 10.1016/j.soildyn.2010.09.009.

J.T. Hewes. 2002. "Seismic Design and Performance of Precast Concrete Segmental Bridge Columns."

Kalkan, Erol, and Sashi K. Kunnath. 2006. "Effects of Fling Step and Forward Directivity on Seismic Response of Buildings." *Earthquake Spectra*. doi: 10.1193/1.2192560.

Kashani, Mohammad M., Ehsan Ahmadi, Alicia Gonzalez-Buelga, Dayi Zhang, and Fabrizio Scarpa. 2019. "Layered Composite Entangled Wire Materials Blocks as Pre-Tensioned Vertebral Rocking Columns." *Composite Structures*. doi: 10.1016/j.compstruct.2019.02.021.

Kashani, Mohammad M., and Alicia Gonzalez-Buelga. 2017. "Nonlinear Dynamics of Self-Centring Segmental Composite Rocking Column." in *Procedia Engineering*.

Kashani, Mohammad M., Alicia Gonzalez-Buelga, Rachael P. Thayalan, Alistair R. Thomas, and Nicholas A. Alexander. 2018. "Experimental Investigation of a Novel Class of Self-Centring Spinal Rocking Column." *Journal of Sound and Vibration*. doi: 10.1016/j.jsv.2018.08.034.

Khoshnoudian, Faramarz, and Ehsan Ahmadi. 2013. "Effects of Pulse Period of Near-Field Ground Motions on the Seismic Demands of Soil-MDOF Structure Systems Using Mathematical Pulse Models." *Earthquake Engineering and Structural Dynamics*. doi: 10.1002/eqe.2287.

Khoshnoudian, Faramarz, Ehsan Ahmadi, and Sina Sohrabi. 2014. "Response of Nonlinear Soil-MDOF Structure Systems Subjected to Distinct Frequency-Content Components of near-Fault Ground Motions." *Earthquake Engineering and Structural Dynamics*. doi: 10.1002/eqe.2367.

Li, Shuai, Taiyi Zhao, M. Shahria Alam, Zhao Cheng, and Jing-quan Wang. 2020. "Probabilistic Seismic Vulnerability and Loss Assessment of a Seismic Resistance Bridge System with Post-Tensioning Precast Segmental Ultra-High Performance Concrete Bridge Columns." *Engineering Structures* 225. doi: 10.1016/j.engstruct.2020.111321.

Makris, N. 2014. "The Role of the Rotational Inertia on the Seismic Resistance of Free-Standing Rocking Columns and Articulated Frames." *Bulletin of the Seismological Society of America* 104(5). doi: 10.1785/0120130064.

Marriott, Dion, Stefano Pampanin, and Alessandro Palermo. 2009. "Quasi-Static and Pseudo-Dynamic Testing of Unbonded Post-Tensioned Rocking Bridge Piers with External Replaceable Dissipaters." *Earthquake Engineering and Structural Dynamics*. doi: 10.1002/eqe.857.

Mavroeidis, G. P., G. Dong, and A. S. Papageorgiou. 2004. "Near-Fault Ground Motions, and the Response of Elastic and Inelastic Single-Degree-of-Freedom (SDOF) Systems." *Earthquake Engineering and Structural Dynamics*. doi: 10.1002/eqe.391.

Mavroeidis, George P., and Apostolos S. Papageorgiou. 2002. "Near-Source Strong Motion: Characteristics and Design Issues." *7th U.S. National Conference on Earthquake Engineering*.

Mavroeidis, George P., and Apostolos S. Papageorgiou. 2003. "A Mathematical Representation of Near-Fault Ground Motions." *Bulletin of the Seismological Society of America*. doi: 10.1785/0120020100.

McKenna, Frank. 2011a. "OpenSees: A Framework for Earthquake Engineering Simulation." *Computing in Science and Engineering*. doi: 10.1109/MCSE.2011.66.

McKenna, Frank. 2011b. "OpenSees: A Framework for Earthquake Engineering Simulation." *Computing in Science and Engineering*. doi: 10.1109/MCSE.2011.66.

Motaref, S. 2011. "Seismic Response of Precast Bridge Columns with Energy Dissipating Joints."

Motaref, Sarira, M. Saiid Saiidi, and David H. Sanders. 2010. "Experimental Study of Precast Bridge Columns with Built-in Elastomer." *Transportation Research Record*. doi: 10.3141/2202-14.

Ou, Yu Chen, Methee Chiewanichakorn, Amjad J. Aref, and George C. Lee. 2007a. "Seismic Performance of Segmental Precast Unbonded Posttensioned Concrete Bridge Columns." *Journal of Structural Engineering*. doi: 10.1061/(ASCE)0733-9445(2007)133:11(1636).

Ou, Yu Chen, Methee Chiewanichakorn, Amjad J. Aref, and George C. Lee. 2007b. "Seismic Performance of Segmental Precast Unbonded Posttensioned Concrete Bridge Columns." *Journal of Structural Engineering*. doi: 10.1061/(ASCE)0733-9445(2007)133:11(1636).

Sehhati, Reza, Adrian Rodriguez-Marek, Mohamed ElGawady, and William F. Cofer. 2011. "Effects of Near-Fault Ground Motions and Equivalent Pulses on Multi-Story Structures." *Engineering Structures*. doi: 10.1016/j.engstruct.2010.11.032.

Sideris, Petros, Amjad J. Aref, and Andre Filiatrault. 2014. "Large-Scale Seismic Testing of a Hybrid Sliding-Rocking Posttensioned Segmental Bridge System." *Journal of Structural Engineering (United States)*. doi: 10.1061/(ASCE)ST.1943-541X.0000961.

Sideris, Petros, Amjad J. Aref, and Andre Filiatrault. 2015. "Experimental Seismic Performance of a Hybrid Sliding-Rocking Bridge for Various Specimen Configurations and Seismic Loading Conditions." *Journal of Bridge Engineering*. doi: 10.1061/(ASCE)BE.1943-5592.0000742.

Spieth HA, Carr AJ, Murahidy AG, Arnolds D, Davies M, and Mander JB. 2004. "Modelling of Post-Tensioned Precast Reinforced Concrete Frame Structures with Rocking Beam-Column Connections." in *New Zealand society of earthquake engineering Conference 2004*.

Tong, Teng, Weiding Zhuo, Xiaofang Jiang, Haipeng Lei, and Zhao Liu. 2019. "Research on Seismic Resilience of Prestressed Precast Segmental Bridge Piers Reinforced with High-Strength Bars through Experimental Testing and Numerical Modelling." *Engineering Structures* 197. doi: 10.1016/j.engstruct.2019.109335.

Vamvatsikos, Dimitrios, and C. Allin Cornell. 2002. "Incremental Dynamic Analysis." *Earthquake Engineering and Structural Dynamics*. doi: 10.1002/eqe.141.

Wang, Jingquan, Zhen Wang, Yuchuan Tang, Tongxu Liu, and Jian Zhang. 2018. "Cyclic Loading Test of Self-Centering Precast Segmental Unbonded Posttensioned UHPFRC Bridge Columns." *Bulletin of Earthquake Engineering*. doi: 10.1007/s10518-018-0331-y.

Wang, Zhen, Jingquan Wang, and Junzheng Zhu. 2018. "Pushover Analysis of Precast Segmental UHPFRC Bridge Columns with Unbonded Posttensioned Tendons." in *Key Engineering Materials*.

Yang, Cancan, Pinar Okumus, and Ruolong Ren. 2019. “A Hysteretic Model for Self-Centering Precast Concrete Piers with Varying Shear-Slip between Segments.” *Engineering Structures* 188. doi: 10.1016/j.engstruct.2019.01.053.

El Zareef, Mohamed, and Mike Schlaich. 2010. “Behaviour of the Joints between Lightweight Concrete Beams and Normal Concrete Columns in Seismic Regions.” in *3rd International fib Congress and Exhibition, Incorporating the PCI Annual Convention and Bridge Conference: Think Globally, Build Locally, Proceedings*.

Zhang, Xihong, and Hong Hao. 2019. “The Response of Precast Concrete Segmental Columns Subjected to near Base Impact.” *International Journal of Protective Structures*. doi: 10.1177/2041419618808534.